European Journal of Radiology 125 (2020) 108825

Contents lists available at ScienceDirect

European Journal of Radiology

journal homepage: www.elsevier.com/locate/ejrad

Research article

Heterogeneity of metastatic gastrointestinal stromal tumor on texture analysis: DWI texture as potential biomarker of overall survival

Jia Fu[a,b,1], Meng-jie Fang[c,d,1], Di Dong[c,d,1], Jian Li[e,1], Ying-shi Sun[a], Jie Tian[c,d,**], Lei Tang[a,*]

[a] Key Laboratory of Carcinogenesis and Translational Research (Ministry of Education/Beijing), Radiology Department, Peking University Cancer Hospital & Institute, Beijing, 100142, China

[b] Department of Radiology, Civil Aviation General Hospital, No. 1 Chaoyang Road, Chaoyang District, Beijing, 100123, China

[c] CAS Key Laboratory of Molecular Imaging, Institute of Automation, Chinese Academy of Sciences, No.95 East Zhongguancun Road, Beijing, 100190, China

[d] University of Chinese Academy of Sciences, Beijing, 100049, China

[e] Key Laboratory of Carcinogenesis and Translational Research (Ministry of Education/Beijing), Departments of Gastroenterology, Peking University Cancer Hospital & Institute, Beijing, 100142, China

ARTICLE INFO

Keywords:
Gastrointestinal stromal tumor
Prognosis
Magnetic resonance imaging
Texture analysis

ABSTRACT

Purpose: To determine if texture features of diffusion weighted imaging (DWI) on MRI of metastatic gastrointestinal stromal tumor (mGIST) have correlation with overall survival (OS).

Method: Fifty-one GIST patients with metastatic lesions who received imatinib targeted therapy were included. Texture features of the largest metastatic lesion were analyzed using inhouse software. Three types of texture features were assessed: fractal features, gray-level co-occurrence matrix (GLCM) features, and gray-level run-length matrix (GLRLM) features. The features were extracted from the regions of interest (ROIs) on T2-weighted imaging (T2WI), DWI and apparent diffusion coefficient (ADC) maps. Histogram analysis was performed on ADC maps. Patients were followed up until death. Kaplan–Meier analysis was performed to determine the correlation of texture features with OS. The curves of the high- and low-risk groups were compared using log-rank test. The prognostic efficacy of the predictors was assessed by calculating the concordance probability.

Results: The median survival time was 43.5 months (range, 3.97–120.90 m). Four DWI and three ADC texture features showed significant correlation with OS on univariate analysis ($p < 0.05$). DWI_L_GLCM_maximum_probability [hazard ratio (HR): 2.062 (1.357–3.131)], ADC_H_GLRLM_mean [HR: 2.174 (1.457–3.244)], and ADC_O_GLCM_cluster_shade [HR: 1.882 (1.324–2.674)] were identified as representative prognostic indicators. The optimum threshold levels for these three features were 1.19×100, 1.71×10 and 2.19×0.1, respectively. Neither histogram analysis values nor fractal features revealed significant correlation with survival status ($p > 0.05$).

Conclusions: Texture features of the mGIST on DWI exhibited correlation with overall survival. High-grade heterogeneity was associated with poor prognosis.

1. Introduction

Gastrointestinal stromal tumor (GIST) is the most common mesenchymal neoplasm arising in the gastrointestinal tract (GI). GIST usually has heterogenous features and may occur anywhere from esophagus to rectum [1]. In a study, 59.9% of patients with localized GIST were cured after initial resection of the primary lesion, while the remaining patients experienced recurrence or metastasis during follow-up [2]. Liver and peritoneum are the most common sites for metastasis [3]. Metastasis is typically associated with poor prognosis, with overall survival (OS) of 24.0–81.3 months [4,5]. There is no consensus on the role of surgery in patients with multifocal progressive disease in the setting of metastatic GIST [6]. Imatinib mesylate has improved the clinical outcomes in this setting [7]. However, there is considerable inter-individual variability in this respect. Some patients experienced rapid progression while others may live for over 10 years with

* Corresponding author at: Key Laboratory of Carcinogenesis and Translational Research (Ministry of Education/Beijing), Radiology Department, Peking University Cancer Hospital & Institute, Beijing, 100142, China.

** Corresponding author at: CAS Key Laboratory of Molecular Imaging, Institute of Automation, Chinese Academy of Sciences, No.95 East Zhongguancun Road, Beijing, 100190, China.

E-mail addresses: jie.tian@ia.ac.cn (J. Tian), tangl@bjcancer.org (L. Tang).

[1] These authors contributed equally to this work.

https://doi.org/10.1016/j.ejrad.2020.108825
Received 4 May 2019; Received in revised form 23 December 2019; Accepted 8 January 2020

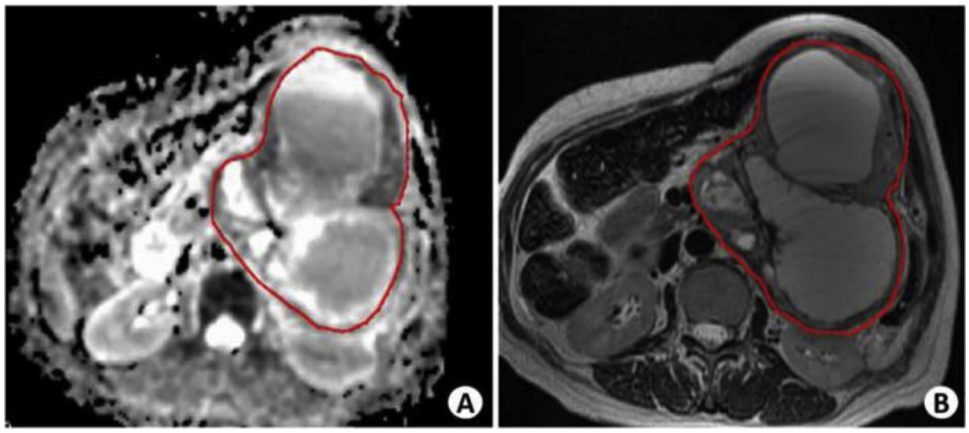

Fig. 1. The region of interest (ROI). (A) The ROIs were drawn on ADC map around the peripheral boundary of the visible tumours in the slice showing the longest dimension using T2WI sequence as a reference. (B) T2WI sequence.

metastatic disease [8].

Texture analysis refers to the extraction and analysis of large amounts of advanced quantitative imaging features with high throughput from medical images obtained with computed tomography (CT), positron emission tomography (PET), or magnetic resonance imaginng (MRI) [9]. This technique has shown good prospects for prognostic assessment, follow-up evaluation, and clinical decision-making. Several studies have validated the prognostic value of texture features in patients with different types of cancer such as metastatic clear cell carcinoma [10], breast cancer [11], and glioblastoma [12]. Recent studies have demonstrated that CT texture analysis may allow for preoperative risk-stratification of patients with primary GIST [13–15]. However, texture analysis has not been used in the context of metastatic GIST. The purpose of this study was to assess the association between texture-derived parameters from DWI and ADC maps and overall survival in patients with mGIST.

2. Methods

2.1. Subjects

This retrospective study enrolled 70 consecutive patients with mGIST from the year 2006 to 2012. Inclusion criteria were: (1) CT proven metastatic GIST (based on typical imaging signs [16,17] with at least one lesion > 1 cm in diameter or cysitic lesions with wall thickness > 1 cm). (2) Suitable for imatinib mesylate monotherapy (400 mg/day, orally). (3) No previous therapy (radiotherapy or chemotherapy) after surgical resection of primary lesion. (4) No contraindications for MR examination. (5) Baseline MRI (include T2WI and DWI sequences) performed in our hospital one week before targeted therapy. (6) Patients with good compliance.

The exclusion criteria were: (1) Previous chemotherapy or other treatment modalities in combination with chemotherapy (n = 1). (2) Discontinued follow-up (n = 4). (3) presence of other tumors (n = 1). (4) Significant artifacts on T2WI and distortion or artifacts on DWI that prevented comparison of the quantitative parameters (n = 1). (5) No available DWI with b = 0, 1000s/mm^2 (n = 12). Finally, 51 patients enrolled in the study.

2.2. MR imaging

The MR examination was performed on 1.5-T scanner (Signa Echo-Speed Plus with EXCITE; GE Medical Systems, Milwaukee, Wisconsin, US). An eight-channel body phase-array surface coil was used to improve the signal-to-noise ratio. All patients underwent MR examination after overnight fasting. In the absence of any contraindications, patients were administered intramuscular injection of anisodamine (20 mg) (Minsheng Pharmaceutical Group, Hangzhou, China) to reduce gastrointestinal motility prior to MR imaging (all patients received the drug eventually). For lesions located in the stomach or duodenum, tap water (800–1000 mL) was administered orally 10 min after the hypotonic procedure, and then the MR examinations were performed.

A full-range abdominal T2-weighted single-shot fast spin-echo sequence (SSFSE: TR/TE, 3000 ms/90 ms; matrix size, 384 × 256; section thickness, 5 mm; intersection gap, 1 mm; field of view, 360–400 mm) on coronary plane was initially performed to detect and locate the lesion. Then axial MR imaging (abdominal and pelvic) was performed, including a T1-weighted dual fast spoiled gradient-recalled echo sequence (dual-FSPGR: TR/TE, 200/2.3 [out-of-phase], 200/4.6 [in-phase]; flip angle, 85°; matrix size, 320 × 160; section thickness, 5 mm; intersection gap, 1 mm; field of view, 360–400 mm; NEX, 1; breath holding) and T2-weighted fast-recovery fast spin-echo sequence (FRFSE: TR/TE, 2 respiratory intervals/85 ms; matrix size, 320 × 224; section thickness, 5 mm; intersection gap, 1 mm; field of view, 360–400 mm; NEX, 2; respiratory triggering).

A single-shot echo-planar DWI sequence (TR/TE, 2750 ms/min; matrix size, 128 × 128; section thickness, 5 mm; intersection gap, 1 mm; field of view, 360–400 mm; NEX, 4) was performed to cover the whole largest lesion. ADC map was generated at high (1000s/mm^2) b values. ADC map was automatically calculated by monoexponential fit.

2.3. Image segmentation

Images were retrieved from the picture archiving and communication system and loaded into ITK–SNAP 2.2.0 software (www.itksnap.org/) for further segmentation. Segmentation was done on the largest slice of the maximum mGIST (J.F. with 3 years of experience on MRI) under the supervision of a board-certified radiologist (L.T. with 16 years of experience on MRI) blinded to the clinical profiles. The largest tumour was defined as the maximum volume among all tumours. The regions of interest (ROI) in the texture analysis was drawn freehand around the peripheral boundary of the maximum tumour by a single observer (Fig. 1). If the tumour was fused, we treated it as one lesion.

The ADC was calculated using the following formula: ADC = [ln (SI $_2$ /SI $_1$)]/(b $_1$—b $_2$), where SI_1 is the signal intensity of the ROI on the b_1 (1000 s/mm ^{2}) image, and SI_2 is the signal intensity of the ROI on the b_2 (0 s/mm^2) image.

2.4. Texture feature extraction

A filtering process was performed to implement image smoothing and image difference (Fig. 2). Separable filtering was used to avoid multi-dimensional convolution. The convolution was performed with a low-/high-pass “Coiflet 1” wavelet filter along x-/y-direction

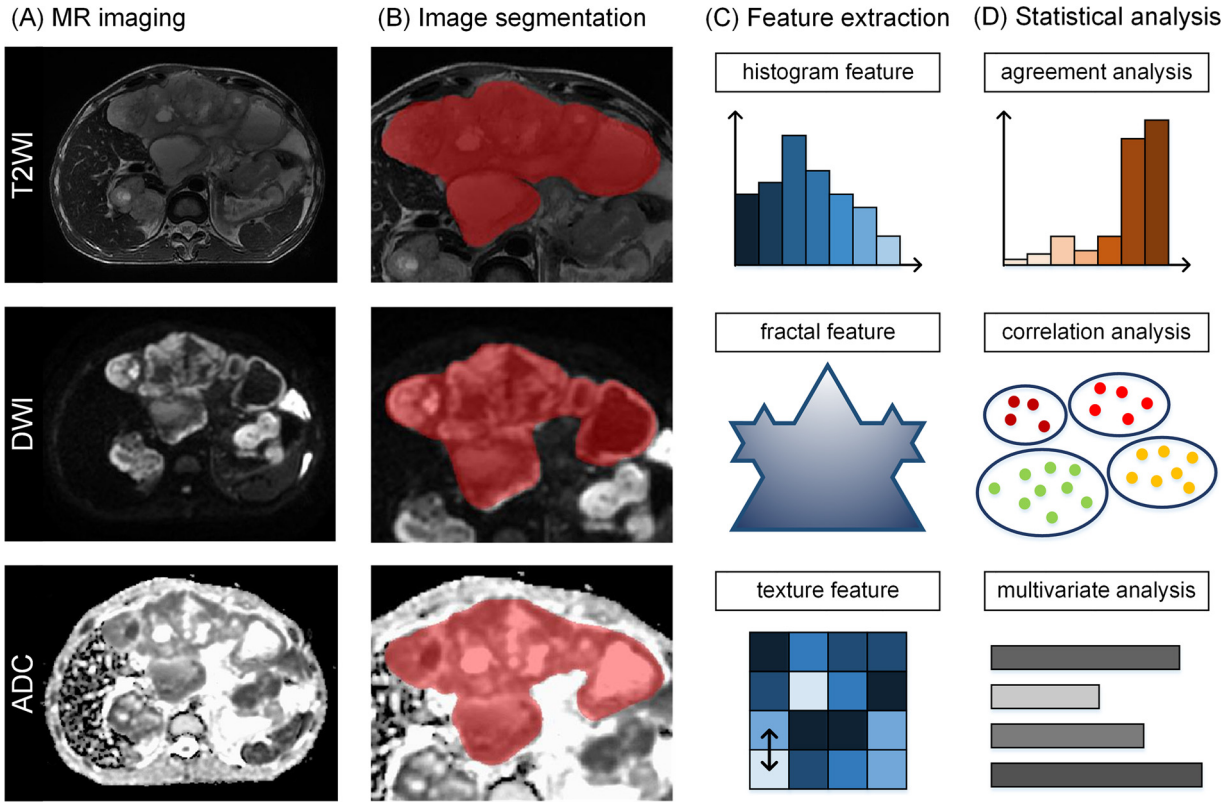

Fig. 2. Schematic diagram for data processing.

separately. That is, two new images were obtained by filtering the original image in two directions (x, y). The original MRI image was labelled as "O", and its low-/high-pass filtered results were labelled as "L" and "H" respectively. One hundred and sixty-seven two-dimensional descriptors were extracted from T2WI, DWI, and ADC images, respectively. They could be divided into gray-level co-occurrence matrix (GLCM) features, gray-level run-length matrix (GLRLM) features and size features. Histogram of ADC values and fractal analysis were also extracted.

2.5. Follow-up

Outpatient records and telephone calls were used for post-treatment follow up of patients every 6 months. The survival time was calculated from the pretreatment of targeted therapy to the time of death.

2.6. Statistical analysis

Firstly, we used the intra-class correlation coefficient (ICC) to evaluate the reader agreement with respect to feature extraction. An ICC > 0.75 was considered indicative of good agreement. The non-reproducible features were removed. Then the Pearson correlation coefficient (hereafter denoted by r) between each pair of features was computed to analyze the linear correlation. The features were divided into different groups to ensure all pairs of features in a group had a |r| value > 0.6. To remove the redundant features, only the most stable feature of each group (with the highest ICC) was retained.

Univariate and multivariate proportional hazard analysis was used to estimate the predictors of end-point events. Backward stepwise selection was applied using the likelihood ratio test with Akaike's information criterion as the stopping rule. We identified the threshold of each significant texture feature for disaggregating patients into high- and low-risk groups using X-Tile. The association of these features with survival was explored with Kaplan–Meier survival analysis. The survival curves of the high- and low-risk groups were compared using the log-rank test. In addition, the prognostic ability of the predictors was assessed by calculating the concordance probability (C-index). P values < 0.05 were considered indicative of statistical significance. All statistical analyses were performed using the R software (version 3.2.5; http://www.Rproject.org).

3. Results

Baseline demographic and clinical data are presented in Table 1. The median survival time was 43.5 months (range, 3.97–120.90months). The 1-year, 2-year, and 3-year survival rates were 78.7 %, 63.6 %, and 27.8 %, respectively.

After assessing the reproducibility, we obtained 128, 113, and 123 robust texture features from T2WI, DWI, and ADC images, respectively (ICC > 0.75 for all). A total of 17, 19, and 20 different groups of correlated features were identified and only the features that exhibited the greatest reproducibility in each group were selected for the subsequent analyses. In our study, four DWI texture features and three ADC texture features showed a significant association with survival on univariate analysis (Table 2). ADC_{mean}, ADC10 %, ADC25 %, ADC75 %, ADC90 %, and fractal feature did not show significant association with survival ($p > 0.05$) (Table 3).

Beginning with the DWI group and the ADC group of significant texture features, backward stepwise selection was implemented. One DWI texture feature (DWI_L_GLCM_maximum_probability) and two ADC texture features (ADC_H_GLRLM_mean and ADC_O_GLCM_cluster_shade) were identified as the representative prognostic indicators for the two MRI sequences, respectively, for the prediction of survival. Subsequently, multivariate proportional hazard analysis demonstrated that all 3 features were independent predictors of survival (Table 4).

The optimum threshold levels for ADC_H_GLRLM_mean, ADC_O_GLCM_cluster_shade, and DWI_L_GLCM_maximum_probability

Table 1
Clinical characteristics.

Characteristics	n = 51
Sex	
Male	28
Female	23
Median age (years)	55 (27–73)
Primary site	
Gastric	27
Small intestine	13
Rectum	3
Other	8
Number of metastasis tumor	
< 5	35
> 5	16
Involved sites	
Liver	13
Peritoneum	10
Liver and Peritoneum	25
Liver and Bone	1
Plevic and Preritoneum	2
Maximum tumor location	
Peritoneum	18
Liver	31
Plecvic	2
Maximum tumor size (cm^2)	44.02 (1.79–167.36)

selected by X-Tile were 1.19 × 100, 1.71 × 10, and 2.19 × 0.1, respectively, for the prediction of five-year survival. Kaplan-Meier curves disaggregated by optimal threshold levels were significantly different for the features with the exception of ADC_O_GLCM_cluster_shade, which yielded a log-rank test P-value of 0.2050. Higher ADC_H_GLRLM_mean and DWI_L_GLCM_maximum_probability were associated with adverse events (Figs. 3 and 4).

4. Discussions

In our study, four DWI texture features and three ADC texture features of mGIST showed significant association with survival. Furthermore, ADC_H_GLRLM_mean, ADC_O_GLCM_cluster_shade, and DWI_L_GLCM_maximum_probability were independent predictors of survival. Texture features calculated based on GLCM or GLRLM are able to depict the contrast, complexity, and the heterogeneity of local intensity patterns. These three independent predictors (one GLRLM feature and two GLCM features) therefore could provide information about tumor heterogeneity and capture the prognostically relevant changes. In our study population, higher average values of metastatic GIST were associated with worse prognosis. The GLRLM feature “mean” tends to emphasize the cluster of short runs and the complicated variation of detailed phenotype patterns. The “maximum probability” of GLCM measures the probability of co-occurrence pairs with the most frequent type, which usually appear around the intensity edge or the uniform interface. The “cluster shade” could be considered as a measure of the skewness of GLCM; it reflects the co-occurrence with large variation and high gray-level. The association between these features and lung cancer was reported from PET/CT study [18].

Table 3
Histogram and fractal analysis features in this study.

Feautres	Mean ± SD	C-index	P-value
$ADC_{10\%}$ (mm^2/sec)	$(1.15 \pm 0.32)\times10^{-3}$	0.383(0.295–0.471)	0.0739
$ADC_{25\%}$ (mm^2/sec)	$(1.34 \pm 0.35)\times10^{-3}$	0.406(0.313–0.499)	0.1315
$ADC_{75\%}$ (mm^2/sec)	$(1.89 \pm 0.82)\times10^{-3}$	0.443(0.339–0.547)	0.2634
$ADC_{90\%}$ (mm^2/sec)	$(2.11 \pm 0.39)\times10^{-3}$	0.426(0.309–0.543)	0.1821
ADC_{mean} (mm^2/sec)	$(1.59 \pm 0.41)\times10^{-3}$	0.423(0.327–0.519)	0.1111
FD	1.95 ± 0.03	0.553(0.442–0.664)	0.1491

SD, standard deviation; ADC, apparent diffusion coefficient; FD,fractal analysis.

Table 4
Results of multivariate analysis of texture features.

Features	Adjusted HR	P-value
ADC_H_GLRLM_mean	2.062 (1.357–3.131)	0.0007
ADC_O_GLCM_cluster_shade	2.174 (1.457–3.244)	0.0001
DWI_L_GLCM_maximum_probability	1.882 (1.324–2.674)	0.0004

HR, hazard ratio; ADC, apparent diffusion coefficient.

Our result is in line with the findings of previous studies and other tumors [19–21]. In a study by Yu et al., presence of intratumorally necrotic changes in primary GISTs showed a correlation with risk of malignancy [19]. Other studies also demonstrated that heterogeneous soft tissue sarcomas were associated with poor prognosis [20,21]. Furthermore, mesenchymal tumors are different from some epithelial tumors. Mesenchymal tumors with poorer outcome tend to undergo necrosis which leads to heterogeneity, while some epithelial tumors with poorer outcome tend to undergo fibrosis which may lead to less heterogeneity/ homogeneity [21,22]. In recent studies, homogenous texture in pancreatic cancer was found associated with worse outcomes owing to the presence of intense intumoral fibrosis (also referred to as desmoplastic reaction) [22,23].

In the present study, no significant difference was found with respect to other parameters, including fractal features, histogram of ADC values and size, on the prediction of five-year survival. However, Kurata et al. showed inconsistent result that fractal analysis might be used to identify high-risk GIST patients [13]. The discrepancy results between their study and ours may be attribute to different patient cohorts. The previous study mainly focused on the primary GIST lesions, yet our study population was composed by metastatic GIST tumors. Theoretically, the cases in our study had relatively poorer prognosis and more prominent heterogeneity, which may need more advanced model for discrimination. Similarly, there was study revealed that lower percentiles of ADC corresponded to the most solid, condense and malignant components in gastric cancer [24]. However, no significant difference in histogram of ADC values was found between different survival status in our mGIST study. We speculate that histogram of ADC values belongs to first-order statistics, which are based on the gray-level frequency distribution and represent a single pixel value rather than its spatial relation to adjacent pixels [25,26], thereafter it might be insufficient for quantification of the overall texture contents in our case of mGIST. Additionally, the largest tumor size of mGIST could not predict

Table 2
Significant texture features identified in this study.

Feautres	Mean ± SD	C-index	HR	P-value
ADC_O_GLRLM_LGLRE	(1.05 ± 1.15)×0.01	0.617 (0.537–0.697)	1.676 (1.202–2.337)	0.0001
ADC_H_GLRLM_mean	(9.38 ± 6.96)×10	0.606 (0.505–0.706)	1.495 (1.041–2.146)	0.0285
ADC_O_GLCM_cluster_shade	(3.64 ± 3.79)×10	0.567 (0.442–0.692)	1.508 (1.016–2.237)	0.0403
DWI_L_GLCM_maximum_probability	(2.08 ± 0.76)×0.1	0.656 (0.572–0.740)	1.762 (1.239–2.505)	0.0015
DWI_L_GLCM_homogeneity	(7.01 ± 0.55)×0.1	0.641 (0.550–0.733)	1.728 (1.117–2.674)	0.0142
DWI_L_GLRLM_LGLRE	(6.97 ± 3.31)×0.01	0.570 (0.456–0.684)	1.544 (1.080–2.208)	0.0173
DWI_L_I_mean_absolute_deviation	(6.10 ± 2.42)×10	0.360 (0.260–0.460)	0.709 (0.516–0.973)	0.0306

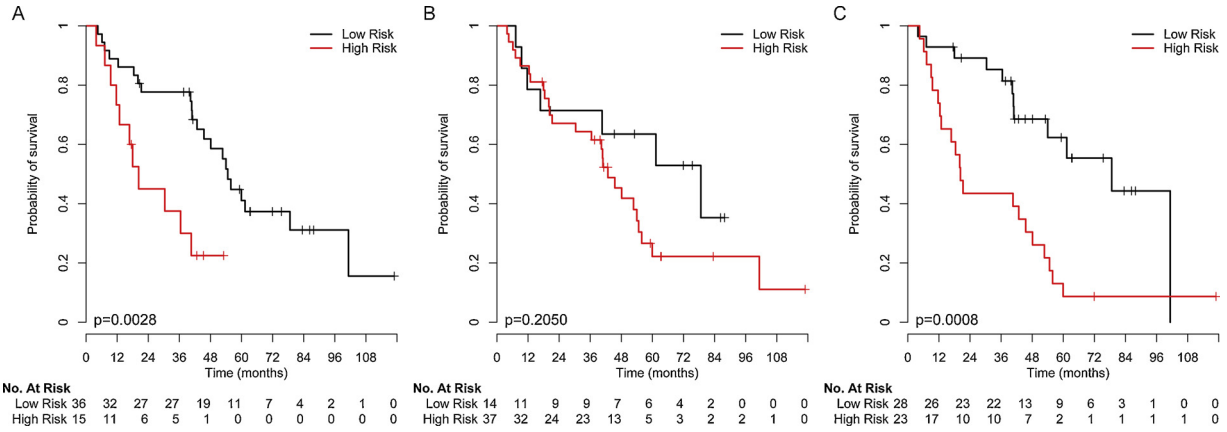

Fig. 3. Kaplan–Meier curves for ADC_H_GLRLM_mean (A), ADC_O_GLCM_cluster_shade (B), and DWI_L_GLCM_maximum_probability (C). For each feature, the optimum threshold point was chosen to divide the entire cohort into two parts. Between-group differences in survival were assessed using the log-rank test.

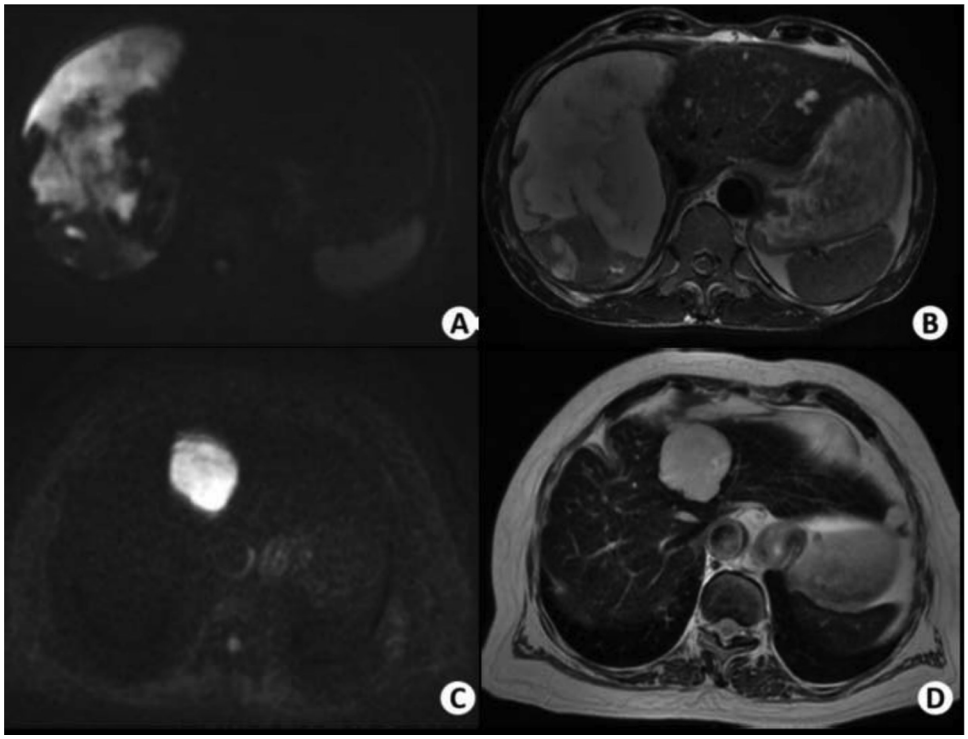

Fig. 4. (A) A 73-year-old male with mGIST in liver and survival time of 7.37 m. Metastatic tumor with high signal on DW imaging (b = 1000sec/mm^2); (B) On T2WI, the tumors exhibit inhomogeneous signal intensity; (C) A 72-year-old male with mGIST in liver and survival time of 56.8 m. Multiple metastatic tumors with high signal on DW imaging (b = 1000sec/mm^2); (D) On T2WI, the tumors exhibit relatively homogeneous signal intensity.

the overall survival, which is similar to the report on the other tumor [22].

There are several limitations in our study. First, the retrospective study design and the relatively small number of patients were the key limitations. Second, only two b values were included (0–1000s/mm^2) on DWI. Application of multiple b values may provide additional information. Becker et al. found that different b values may lead to variability in texture analysis [27]. Third, we investigated the largest metastatic lesion to perform analysis rather than all visible metastases, for the convenience of clinical practice; this may introduce bias [15,28]. Fourth, we did not assess interobserver variability. Finally, future studies should combine more imaging parameters and clinical information to generate more efficient models.

5. Conclusion

Imaging features of metastatic GIST on DWI were independently associated with survival, which suggests the need for further validation of texture analysis as a potential biomarker. High-grade heterogeneity was associated with poor prognosis.

Ethical standards

All human and animal studies have been approved by the appropriate ethics committee and have therefore been performed in accordance with the ethical standards laid down in the 1964 Declaration of Helsinki and its later amendments or comparable ethical standards.

Informed consent

All patients gave their informed consent prior to their inclusion in the study.

Declaration of Competing Interest

The Authors declare that they have no conflict of interest.

Acknowledgments

National Key R&D Program of China (No. 2018YFC0910700, 2017YFC1309101, 2017YFC1309104); Beijing Natural Science Foundation (No. Z180001, L182061); National Natural Science Foundation of China (91959130, 81971776, 81771924).

References

[1] M. Miettinen, J. Lasota, Gastrointestinal stromal tumors: pathology and prognosis at different sites, Semin. Diagn. Pathol. 23 (2006) 70–83.
[2] H. Joensuu, A. Vehtari, J. Riihimäki, et al., Risk of recurrence of gastrointestinal stromal tumour after surgery: an analysis of pooled population-based cohorts, Lancet Oncol. 13 (2012) 265–274, https://doi.org/10.1016/S1470-2045(11)70299-6.
[3] H. Joensuu, J. Martin-Broto, T. Nishida, et al., Follow-up strategies for patients with gastrointestinal stromal tumour treated with or without adjuvant imatinib after surgery, Eur. J. Cancer 51 (2015) 1611–1617, https://doi.org/10.1016/j.ejca.2015.05.009.
[4] W.T.A. van der Graaf, R. Tielen, J.J. Bonenkamp, et al., Nationwide trends in the incidence and outcome of patients with gastrointestinal stromal tumour in the imatinib era, Br. J. Surg. 105 (2018) 1020–1027, https://doi.org/10.1002/bjs.10809.
[5] C.D. Blanke, G.D. Demetri, M. von Mehren, et al., Long term results from a randomized phase II trial of standardversus higher-dose imatinib mesylate for patients with unresectable or metastatic gastrointestinal stromal tumors expressing KIT, J. Clin. Oncol. 26 (2008) 620–625, https://doi.org/10.1200/JCO.2007.13.4403.
[6] S.J. Ford, A. Gronchi, Indications for surgery in advanced/metastatic GIST, Eur. J. Cancer 63 (2016) 154–167, https://doi.org/10.1016/j.ejca.2016.05.019.
[7] S. Sleijfer, E. Wiemer, J. Verweij, Drug Insight: gastrointestinal stromal tumors (GIST) the solid tumor model for cancer-specific treatment, Nat. Clin. Pract. Oncol. 5 (2008) 102–111, https://doi.org/10.1038/ncponc1037.
[8] A.K. Dip Borunda, A. Pimentel Renteria, M. Pluma Jiménez, et al., Treatment of non-resectable and metastatic gastrointestinal stromal tumors: experience with the use of tyrosine kinase inhibitors in a third level hospital in Mexico, J. Clin. Oncol. 7 (2016) 632–637, https://doi.org/10.21037/jgo.2016.06.03.
[9] P. Lambin, E. Rios-Velazquez, R. Leijenaar, et al., Radiomics: extracting more information from medical images using advance feature analysis, Eur. J. Cancer 48 (2012) 441–446, https://doi.org/10.1016/j.ejca.2011.11.036.
[10] M.A. Haider, A. Vosough, F. Khalvati, et al., CT texture analysis: a potential tool for prediction of survival in patients with metastatic clear cell carcinoma treated with sunitinib, Cancer Imaging 17 (2017) 4, https://doi.org/10.1186/s40644-017-0106-8.
[11] J.H. Kim, E.S. Ko, Y. Lim, et al., Breast Cancer heterogeneity:MR imaging texture analysis and survival outcomes, Radiology 282 (2017) 665–675, https://doi.org/10.1148/radiol.2016160261.
[12] P. Kickingereder, S. Burth, A. Wick, et al., Radiomic profiling of glioblastoma: identifying an imaging predictor of patient survival with improved performance over established clinical and radiologic risk models, Radiology 280 (2016) 880–889, https://doi.org/10.1148/radiol.2016160845.
[13] Y. Kurata, K. Hayano, G. Ohira, et al., Fractal analysis of contrast-enhanced CT images for preoperative prediction of malignant potential of gastrointestinal stromal tumor, Abdom Radiol (NY). 43 (2018) 2659–2664, https://doi.org/10.1007/s00261-018-1526-z.
[14] T. Chen, Z. Ning, L. Xu, et al., Radiomics nomogram for predicting the malignant potential of gastrointestinal stromal tumours preoperatively, Eur. Radiol. 29 (2019) 1074–1082, https://doi.org/10.1007/s00330-018-5629-2.
[15] F. Xu, X. Ma, Y. Wang, et al., CT texture analysis can be a potential tool to differentiate gastrointestinal stromal tumors without KIT exon 11 mutation, Eur. J. Radiol. 107 (2018) 90–97, https://doi.org/10.1016/j.ejrad.2018.07.025.
[16] S. Bano, S.K. Puri, L. Upreti, et al., Gastrointestinal stromal tumors (GISTs): an imaging perspective, J. Radiol. 30 (2012) 105–115, https://doi.org/10.1007/s11604-011-0020-0.
[17] Y.M. ElGuindy, S. Javadi, C.O. Menias, et al., Imaging of secretory tumors of the gastrointestinal tract, Abdom Radiol (NY). 42 (2017) 1350, https://doi.org/10.1007/s00261-016-0976-4.
[18] M. Kirienko, L. Cozzi, L. Antunovic, et al., Prediction of disease-free survival by the PET/CT radiomic signature in non-small cell lung cancer patients undergoing surgery, Eur. J. Nucl. Med. Mol. Imaging 45 (2017) 207–217, https://doi.org/10.1007/s00259-017-3837-7.
[19] L.J.M. Yu MH, J.H. Baek, J.K. Han, B.I. Choi, MRI features of gastrointestinal stromal tumors, AJR Am. J. Roentgenol. 203 (2014) 980–991, https://doi.org/10.2214/AJR.13.11667.
[20] K. Hayano, F. Tian, A.R. Kambadakone, S.S. Yoon, et al., Texture analysis of non-contrast-Enhanced computed tomography for assessing angiogenesis and survival of Soft tissue sarcoma, J. Comput. Assist. Tomogr. 39 (2015) 607–612, https://doi.org/10.1097/RCT.0000000000000239.
[21] M. Malek, M. Rahmani, S.M. Seyyed Ebrahimi, et al., Investigating the diagnostic value of quantitative parameters based on T2-weighted and contrast-enhanced MRI with psoas muscle and outer myometrium as internal references for differentiating uterine sarcomas from leiomyomas at 3T MRI, Cancer Imaging 19 (2019) 20, https://doi.org/10.1186/s40644-019-0206-8.
[22] K. Sandrasegaran, Y. Lin, M. Asare-Sawiri, et al., CT texture analysis of pancreatic caner, Eur. Radiol. 29 (2019) 1067–1073, https://doi.org/10.1007/s00330-018-5662-1.
[23] G. Yun, Y.H. Kim, Y.J. Lee, et al., Tumor heterogeneity of pancreas head cancer assessed by CT texture analysis: association with survival outcomes after curative resection, Sci. Rep. 8 (2018) 7226, https://doi.org/10.1038/s41598-018-25627-x.
[24] S. Liu, Y. Zhang, L. Chen, et al., Whole-lesion apparent diffusion coefficient histogram analysis: significance in T and N staging of gastric cancers, BMC Cancer 17 (2017) 665, https://doi.org/10.1186/s12885-017-3622-9.
[25] L. Brenet Defour, S. Mulé, A. Tenenhaus, et al., Hepatocellular carcinoma: CT texture analysis as a predictor of survival after surgical resection, Eur. Radiol. 29 (2019) 1231–1239, https://doi.org/10.1007/s00330-018-5679-5.
[26] B.R. Kim, J.H. Kim, S.J. Ahn, et al., CT prediction of resectability and prognosis in patients with pancreatic ductal adenocarcinoma after neoadjuvant treatment using image findings and texture analysis, Eur. Radiol. 29 (2019) 362–372, https://doi.org/10.1007/s00330-018-5574-0.
[27] A.S. Becker, M.W. Wagner, M.C. Wurnig, A. Boss, Diffusion-weighted imaging of the abdomen: impact of b-values on texture analysis features, NMR Biomed. 30 (2017), https://doi.org/10.1002/nbm.3669.
[28] D. Dong, L. Tang, Z.Y. Li, et al., Development and validation of an individualized nomogram to identify occult peritoneal metastasis in patients with advanced gastric cancer, Ann. Oncol. 30 (2019) 431–438, https://doi.org/10.1093/annonc/mdz001.